Mechanics of Advanced Composite Structures 4 (2017) 153-168

Semnan University

Mechanics of Advanced Composite Structures

journal homepage: http://MACS.journals.semnan.ac.ir

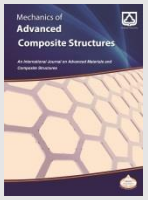

Mesh-free Dynamic Analyses of FGM Sandwich Plates Resting on A Pasternak Elastic Foundation

R. Moradi-Dastjerdi [a*], H. Momeni-Khabisi [b], R. Baghbani [c]

[a] *Young Researchers and Elite Club,Khomeinishahr Branch, Islamic Azad University, Khomeinishahr, Iran*
[b] *Department of Mechanical Engineering, University of Jiroft, Jiroft, Iran*
[c] *Department of Water Engineering, Isfahan University of Technology, Isfahan, Iran*

PAPER INFO

Paper history:
Received 2017-04-13
Revised 2017-05-12
Accepted 2017-06-03

Keywords:
Wave propagation
Sandwich plate
Functional graded material
Mesh-free
First-order shear deformation theory

ABSTRACT

This study analyzes the free vibration, forced vibration, resonance, and stress wave propagation of orthotropic sandwich plates made of functionally graded materials (FGMs). Dynamic analyses are conducted using a mesh-free method based on first-order shear deformation theory and the shape functions constructed using moving least squares approximation. The sandwich plates are rested on a Pasternak elastic foundation and subjected to periodic or impact loading and essential boundary conditions, which are imposed through a transfer function method. The sandwich plates are assumed to be composed of a homogeneous orthotropic core and two orthotropic FGM face sheets made of two orthotropic materials. The volume fractions of the materials are varied smoothly along the thickness of the face sheets. The convergence and accuracy of the applied method are demonstrated, after which numerical analyses are conducted to investigate the effects of elastic foundation coefficients, material distributions, geometrical dimensions, time-dependent loading, and boundary conditions on the vibrational and dynamic characteristics of the orthotropic FGM sandwich plates.

DOI: 10.22075/MACS.2017.11043.1107

1. INTRODUCTION

A new class of materials known as functionally graded materials (FGMs) have attracted considerable attention as advanced structural materials for many structural members. FGMs are heterogeneous composite materials with gradient compositional variations in their constituents (e.g., metal and ceramic) from one surface of the materials to another. These variations result in continuously varying material properties. The materials are designed in such a way that they possess desirable properties for specific applications. The concept of FGMs, initially developed for superheat-resistant materials for use in space planes or nuclear fusion reactors, is currently of interest to designers of functional materials for energy converters, dental and orthopedic implants, sensors, and thermogenerators [1]. Generally, numerous engineering problems can be modeled as thick plates on elastic foundations, such as the mat foundations of buildings, the pavement underneath roads, and the bases of heavy machines. The mechanical behavior of elastic foundations was widely discussed by Winkler [2] as a one-parameter model or linear model and by Pasternak [3] as a two-parameter model.

Two-dimensional plate theories, including classical plate theory (CPT), first-order shear deformation theory (FSDT), and higher-order shear deformation theories (HSDTs), are commonly used in plate analysis. CPT provides reasonable results for thin plates, but it neglects transverse shear deformation effects, underestimates deflections, and overestimates frequencies, as well as the buckling loads of moderately thick plates [4]. To overcome the limitations of CPT, researchers have developed many shear deformation plate theories that account for transverse shear deformation effects. The theories put forward by Reissner [5] and Mindlin [6] are known as FSDTs. FSDT provides a sufficiently accurate description of response for thin to moderately thick plates [7]. It is widely used in the finite element analyses of composite shells and plates be-

* Corresponding author. Tel.: +98-913-2058928, Fax: +98-31-33660088

E-mail address: rasoul.moradi@iaukhsh.ac.ir

cause of its acceptable accuracy and computational complexity [9–11]. However, its performance strongly depends on shear correction factors, which are sensitive not only to material and geometric properties but also to loading and boundary conditions. To avoid the use of shear correction factors and include the actual cross-section warping of a plate into analyses, scholars extensively developed HSDTs, with consideration for the higher-order variations in in-plane displacement throughout the thickness of plates [8].

Aiello and Ombres [12] presented an analytical approach to evaluating the buckling load of sandwich panels made of hybrid laminated faces and a transversely flexible core. The authors applied the a priori assumption of the displacement field throughout the thickness of the panels; that is, the authors superpositioned symmetric and anti-symmetric components, aside from adopting a pure compressive mode. Ferreira et al. [13] presented the static deformations and free vibrations of shear flexible isotropic and laminated composite plates with an FSDT theory based on a high-order collocation method. They also analyzed isotropic and laminated plates by using Kansa's non-symmetric radial basis function collocation method, which is based on an HSDT [14]. Shariyat [15] investigated the effects of thermo-piezoelasticity on dynamic buckling under suddenly applied thermal and mechanical loads for imperfect rectangular composite plates with surface-bonded or embedded piezoelectric sensors and actuators. The author developed a finite element formulation grounded in an HSDT and considered the temperature dependence of material properties. Other researchers used HSDT and the general von Karman equation as bases in analyzing the nonlinear vibration and dynamic response of an FGM plate with piezoelectric actuators [16] and surface-bonded piezoelectric fiber-reinforced composite actuators [17]. Malekzadeh et al. [18] investigated the dynamic response of thick laminated annular sector plates with simply supported radial edges subjected to a radially distributed line load moving along the circumferential direction. The authors used a three-dimensional (3D) hybrid method composed of a series solution, layerwise theory, and a differential quadrature method (DQM), in conjunction with the finite difference method. Zhang et al. [19] employed Reddy's third-order shear deformation theory and the Galerkin procedure in determining the non-linear dynamics and chaos that underlie a simply supported orthotropic FGM rectangular plate in a thermal environment. The researchers subjected the plate to parametric and external excitations. Dehghan and Baradaran [20] used a combination of finite element methods and DQMs to solve the eigenvalue (buckling and free vibration) equations of rectangular thick plates resting on Pasternak elastic foundations. Thai and Choi [21, 22] developed a refined plate theory for the free vibration and buckling analyses of FGM plates resting on an elastic foundation. Asemi and Shariyat [23] developed a highly accurate non-linear 3D energy-based finite element elasticity formulation for the buckling investigation of anisotropic FGM plates with arbitrary orthotropic directions. To achieve the most accurate results, the authors used a fully compatible Hermitian element with 168 degrees of freedom, which satisfies the continuity of strain and stress components at the mutual edges and nodes of the element a priori. Mansouri and Shariyat [24] conducted a thermo-mechanical buckling analysis of orthotropic auxetic plates (with negative Poisson ratios) resting on an elastic foundation in hygrothermal environments. Shariyat and Asemi [25] used a non-linear finite element method and 3D elasticity theory to probe into the shear buckling of orthotropic heterogeneous FGM plates resting on a Winkler elastic foundation. Sofiyev et al. [26] presented analytical formulations and solutions for the stability analysis of heterogeneous orthotropic truncated conical shells subjected to external (lateral and hydrostatic) pressures with mixed boundary conditions. For this purpose, the researchers used Donnell shell theory. Furthermore, the vibrational behavior of single- or multi-directional FGMs and functionally graded carbon nanotube-reinforced composite (FG-CNTRC) structures was investigated using 3D elasticity theory and generalized DQM [27–35].

Some forms of the mesh-free method were used to analyze FGM structures. Qian et al. [36] inquired into the static, free, and forced vibrations of a thick rectangular FGM plate on the basis of higher-order shear and normal deformation theory and a meshless local Petrov–Galerkin (MLPG) method. Liew et al. [37] investigated the active control of laminated composite plates with piezoelectric sensor/actuator patches by employing an element-free Galerkin (EFG) method and FSDT. They used a simple control algorithm to regulate the dynamic response of laminated plates with distributed sensor/actuator patches through a closed control loop. Lanhe et al. [38] examined the dynamic stability of thick FGM plates subjected to aero-thermomechanical loads by using a moving least squares DQM. Rezaei Mojdehi et al. [39] carried out a 3D static and dynamic analysis of thick isotropic FGM plates on the basis of MLPG, which is used to construct 3D moving least squares shape functions. The static deformation, free vibration, and dynamic and stress wave propagation of FGM cylinders were analyzed using the same mesh-free method adopted in the current research [40–42]. In these previous works, however,

the structures examined were axisymmetric and isotropic cylinders. Lei et al. [43, 44] analyzed the buckling and free vibration of FG-CNTRC plates by using the element-free kp-Ritz method based on FSDT. Moradi-Dastjerdi et al. [45–47] carried out a dynamic analysis of functionally graded nanocomposite cylinders. The authors also analyzed the static, vibrational, and dynamic behaviors of functionally graded nanocomposite plates reinforced by wavy nanotubes through the same mesh-free method adopted in the present study. In an absorbing work, Yaghoubshahi and Alinia [48] developed an EFG method based on HSDT to eliminate transverse shear locking in the analysis of laminated composite plates. The authors compared their results with those obtained using an EFG procedure based on FSDT. Finally, Zhang et al. [49, 50] proposed an element-free-based improved moving least squares-Ritz method and FSDT to study the buckling behavior of FG-CNTRC plates resting on Winkler foundations. The authors also examined the non-linear bending of the plates as they rested on a two-parameter elastic foundation.

As can be seen in the discussion above, no study has been devoted to the analysis of the free vibration, forced vibration, resonance, and stress wave propagation of orthotropic FGM sandwich plates subjected to periodic or impact loading. To address this deficiency, the present research develops a mesh-free method on the basis of FSDT to investigate the dynamic behaviors of orthotropic FGM sandwich plates resting on a two-parameter Pasternak elastic foundation. In the mesh-free method, shape functions constructed through a moving least squares method are used to approximate the displacement field in the weak form of a motion equation. A transfer function method is employed in the implementation of essential boundary conditions. The developed method does not increase calculations against EFG [41]. The orthotropic FGM sandwich plates are assumed to be composed of two orthotropic FGM face sheets and a homogeneous orthotropic core. The face sheets are assumed to be made of two orthotropic materials, whose volume fractions are varied smoothly along the thickness of the face sheets. The study also examines the effects of elastic foundation coefficients, material distributions, sandwich plate thickness, face sheet thickness, plate aspect ratio, and time-dependent force and boundary conditions on the free vibration, forced vibration, resonance, and stress wave propagation of the plates.

2. MATERIAL PROPERTIES OF ORTHOTROPIC FGM PLATES

Let us consider an orthotropic sandwich FGM plate of length a, width b, total thickness h, and face sheet thickness h_f. The material composition of the plate is shown in Fig. 1. The material properties of the face sheets are assumed to be graded along the thickness of the sheets. The profile of this variation exerts important effects on plate behavior. Several models have been proposed for variations in material properties. Among these, the volume fraction model is the most frequently used. In this model, the volume fraction and material properties of a sandwich plate are varied as follows:

$$\begin{cases} V_2 = (1-\dfrac{h-2z}{2h_f})^n & \text{for top face} \\ V_2 = 0 & \text{for core} \\ V_2 = (1-\dfrac{h+2z}{2h_f})^n & \text{for bottom face} \end{cases} \quad (1)$$

$$P(z) = P_1 + (P_2 - P_1)V_2 \quad (2)$$

where P is an indicator of the material properties of a plate; this indicator is used in lieu of modulus elasticity E, Poisson's ratio υ, and density ρ. Subscripts 1 and 2 represent the z=0 and z=h constituents, respectively; and n denotes the volume fraction exponent. An n equal to zero represents a sandwich plate made of two different materials in the face sheets and a core without any mixture of materials. By contrast, an infinite n indicates a homogeneous plate made of core constituents. Fig. 2 illustrates the variations in the material volume fraction of the FGM sandwich plate along the thickness of the plate at different volume fraction exponents.

3. GOVERNING EQUATIONS

On the basis of FSDT, displacement components can be defined as [4]

$$\begin{aligned} u(x,y,z) &= u_0(x,y) + z\theta_x(x,y) \\ v(x,y,z) &= v_0(x,y) + z\theta_y(x,y) \\ w(x,y,z) &= w_0(x,y) \end{aligned} \quad (3)$$

where u, v, and w are displacements in the x, y, and z directions, respectively; u_0, v_0, and w_0 denote the mid-plane displacements and the θ_x and θ_y rotations of the normal to the mid-plane directions about the y-axis and x-axis, respectively. Kinematic relations can be obtained as follows:

$$\begin{bmatrix} \varepsilon_{xx} & \varepsilon_{yy} & \gamma_{xy} \end{bmatrix}^T = \boldsymbol{\varepsilon}_0 + z\boldsymbol{\kappa}, \begin{bmatrix} \gamma_{yz} & \gamma_{xz} \end{bmatrix}^T = \boldsymbol{\gamma}_0 \quad (4)$$

where

$$\boldsymbol{\varepsilon}_0 = \begin{Bmatrix} \partial u_0/\partial x \\ \partial v_0/\partial y \\ \partial u_0/\partial y + \partial v_0/\partial x \end{Bmatrix}, \boldsymbol{\kappa} = \begin{Bmatrix} \partial \theta_x/\partial x \\ \partial \theta_y/\partial y \\ \partial \theta_x/\partial y + \partial \theta_y/\partial x \end{Bmatrix} \quad (5)$$

$$\boldsymbol{\gamma}_0 = \begin{Bmatrix} \partial v/\partial z + \partial w/\partial y \\ \partial u/\partial z + \partial w/\partial x \end{Bmatrix} = \begin{Bmatrix} \varphi_y + \partial w_0/\partial y \\ \varphi_x + \partial w_0/\partial x \end{Bmatrix}$$

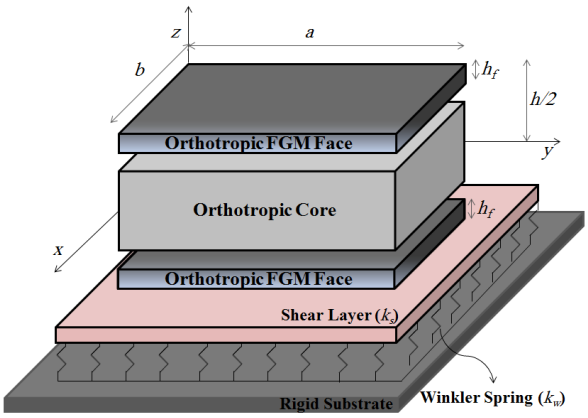

Figure 1 Schematic of orthotropic FGM sandwich plate resting on Pasternak elastic foundation

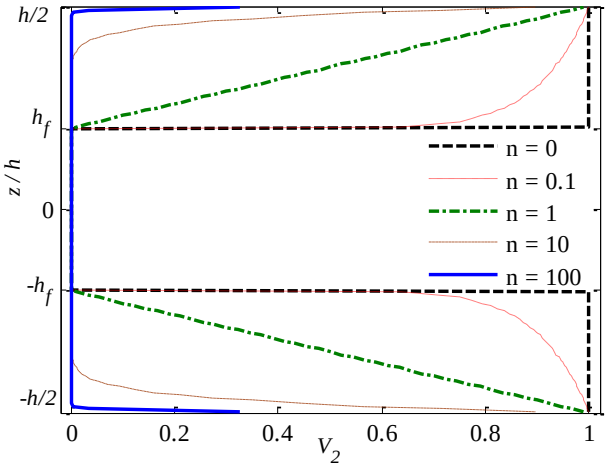

Figure 2 Variations in material volume fraction of orthotropic FGM sandwich plate along the plate thickness at different volume fraction exponents

The linear constitutive relations of a functionally graded plate can be written as

$$\begin{Bmatrix}\sigma_x\\ \sigma_y\\ \sigma_{xy}\end{Bmatrix}=\begin{Bmatrix}Q_{11}(z) & Q_{12}(z) & 0\\ Q_{12}(z) & Q_{22}(z) & 0\\ 0 & 0 & Q_{66}(z)\end{Bmatrix}\begin{Bmatrix}\varepsilon_x\\ \varepsilon_y\\ \varepsilon_{xy}\end{Bmatrix} \quad \text{or } \boldsymbol{\sigma}=\mathbf{Q}_b\boldsymbol{\varepsilon} \tag{6}$$

$$\begin{Bmatrix}\sigma_{yz}\\ \sigma_{xz}\end{Bmatrix}=\alpha(z)\begin{bmatrix}Q_{44}(z) & 0\\ 0 & Q_{55}(z)\end{bmatrix}\begin{Bmatrix}\varepsilon_{yz}\\ \varepsilon_{xz}\end{Bmatrix} \text{ or } \boldsymbol{\tau}=\alpha(z)\mathbf{Q}_s\boldsymbol{\gamma}$$

in which $\boldsymbol{\sigma}$, $\boldsymbol{\tau}$, $\boldsymbol{\varepsilon}$, $\boldsymbol{\gamma}$, and Q_{ij} are the normal stress vector, shear stress vector, normal strain vector, shear strain vector, and engineering constants, respectively. α denotes the transverse shear correction coefficient, which is set at $\alpha=5/6$ for homogeneous materials and $\alpha=5/(6-(\upsilon_1V_1+\upsilon_2V_2))$ for FGMs (where $\upsilon=\upsilon_{12}$ for orthotropic FGM structures) [51]. In Eq. (6), as well,

$$Q_{11}=\frac{1-\nu_{23}\nu_{32}}{E_2E_3\Delta},\ Q_{22}=\frac{1-\nu_{31}\nu_{13}}{E_1E_3\Delta},$$
$$Q_{12}=\frac{\nu_{21}+\nu_{31}\nu_{23}}{E_2E_3\Delta} \tag{7}$$
$$Q_{44}=G_{23},\ Q_{55}=G_{31},\ Q_{66}=G_{12}$$
$$\Delta=\frac{1-\nu_{32}\nu_{23}-\nu_{21}\nu_{12}-\nu_{13}\nu_{31}-2\nu_{32}\nu_{21}\nu_{13}}{E_1E_2E_3}$$

Considering the Pasternak foundation model, the total energy of the plate is expressed thus:

$$U=\frac{1}{2}\int_V\left[\boldsymbol{\varepsilon}^T\boldsymbol{\sigma}+\boldsymbol{\gamma}^T\boldsymbol{\tau}-\rho(z)(\dot{u}^2+\dot{v}^2+\dot{w}^2)\right]dV$$
$$+\frac{1}{2}\int_A\left[k_ww^2+k_s\left[\left(\frac{\partial w}{\partial x}\right)^2+\left(\frac{\partial w}{\partial y}\right)^2\right]\right]dA \tag{8}$$
$$+\int_A[q(t)w]dA$$

where $q(t)$ is the time-dependent applied load, and k_w and k_s are the coefficients of Winkler and Pasternak (shear) foundations, respectively. If a foundation is modeled as a linear Winkler foundation, the coefficient k_s in Eq. (8) takes the value of zero.

4. MESH-FREE NUMERICAL ANALYSES

In these analyses, the moving least squares shape functions introduced by Lancaster and Salkauskas [52] are used to approximate the displacement vector in the weak form of a motion equation. Displacement vector $\mathbf{u}$ can be approximated using the shape functions as follows:

$$\hat{\mathbf{d}}=\sum_{i=1}^{N}\phi_i d_i \tag{9}$$

where N is the total number of nodes, $\hat{\mathbf{d}}$ denotes the virtual nodal values vector, and ϕ_i is the moving least squares shape function of the node located at $\mathbf{X}(x,y)=\mathbf{X}_i$. These variables are defined in the following manner:

$$\hat{\mathbf{d}}=\left[\hat{u}_i,\hat{v}_i,\hat{w}_i,\hat{\theta}_{x_i},\hat{\theta}_{y_i}\right]^T \tag{10}$$

and

$$\phi_i(\mathbf{X})=\underbrace{\mathbf{P}^{\mathbf{T}}(\mathbf{X})[\mathbf{H}(\mathbf{X})]^{-1}W(\mathbf{X}-\mathbf{X}_i)\mathbf{P}(\mathbf{X}_i)}_{(1\times1)} \tag{11}$$

In Eq. (11), W is the cubic spline weight function, $\mathbf{P}$ is the base vector, and $\mathbf{H}$ is the moment matrix. These are defined thus:

$$\mathbf{P}(\mathbf{X})=[1,x,y]^T \tag{12}$$

$$\mathbf{H}(\mathbf{X})=\left[\sum_{i=1}^{n}W(\mathbf{X}-\mathbf{X}_i)\mathbf{P}(\mathbf{X}_i)\mathbf{P}^{\mathbf{T}}(\mathbf{X}_i)\right] \tag{13}$$

Using the moving least squares shape function enables Eq. (4) to be written as

$$\boldsymbol{\varepsilon}=\mathbf{B}_m\hat{\mathbf{d}}+z\mathbf{B}_b\hat{\mathbf{d}}\ ,\ \boldsymbol{\gamma}=\mathbf{B}_s\hat{\mathbf{d}} \tag{14}$$

in which

$$\mathbf{B}_m=\begin{bmatrix}\phi_{i,x} & 0 & 0 & 0 & 0\\ 0 & \phi_{i,y} & 0 & 0 & 0\\ \phi_{i,y} & \phi_{i,x} & 0 & 0 & 0\end{bmatrix},$$
$$\mathbf{B}_b=\begin{bmatrix}0 & 0 & 0 & \phi_{i,x} & 0\\ 0 & 0 & 0 & 0 & \phi_{i,y}\\ 0 & 0 & 0 & \phi_{i,y} & \phi_{i,x}\end{bmatrix}, \quad (15)$$
$$\mathbf{B}_s=\begin{bmatrix}0 & 0 & \phi_{i,x} & \phi_i & 0\\ 0 & 0 & \phi_{i,y} & 0 & \phi_i\end{bmatrix}$$

For an elastic foundation, $\boldsymbol{\varphi}_w$ and $\mathbf{B}_p$ can be defined as follows:

$$\boldsymbol{\varphi}_w=\begin{bmatrix}0 & 0 & \phi_i & 0 & 0\end{bmatrix},$$
$$\mathbf{B}_p=\begin{bmatrix}0 & 0 & \phi_{i,x} & 0 & 0\\ 0 & 0 & \phi_{i,y} & 0 & 0\end{bmatrix} \quad (16)$$

Substituting Eqs. (6) and (14) into Eq. (8) yields

$$U=\frac{1}{2}\int_A\hat{\mathbf{d}}\int_z(\mathbf{B}_m^T\mathbf{A}\mathbf{B}_m+\mathbf{B}_m^T\overline{\mathbf{B}}\mathbf{B}_b+\mathbf{B}_b^T\overline{\mathbf{B}}\mathbf{B}_m+\mathbf{B}_b^T\mathbf{D}\mathbf{B}_b+\mathbf{B}_s^T\mathbf{A}_s\mathbf{B}_s)dz\hat{\mathbf{d}}dA-\frac{1}{2}\int_A\ddot{\hat{\mathbf{d}}}\int_z\left[\mathbf{G}_i^T\overline{\mathbf{M}}\mathbf{G}_j\right]dz\ddot{\hat{\mathbf{d}}}dA+\frac{1}{2}\int_A\left[\boldsymbol{\varphi}_w^Tk_w\boldsymbol{\varphi}_w+\mathbf{B}_p^Tk_s\mathbf{B}_p\right]\hat{\mathbf{d}}dA+\frac{1}{2}\int_A\boldsymbol{\varphi}_w^Tq(t)dA \quad (17)$$

in which the components of extensional stiffness $\mathbf{A}$, bending-extensional coupling stiffness $\overline{\mathbf{B}}$, bending stiffness $\mathbf{D}$, transverse shear stiffness $\mathbf{A}_s$, and $\mathbf{G}_i$ and $\overline{\mathbf{M}}$ are introduced into a mass matrix. These variables are defined as

$$(\mathbf{A},\overline{\mathbf{B}},\mathbf{D})=\int_{-h/2}^{h/2}\mathbf{Q}_b(1,z,z^2)dz\ ,\quad \mathbf{A}_s=\alpha\int_{-h/2}^{h/2}\mathbf{Q}_s dz \quad (18)$$

and

$$\mathbf{G}_i=\begin{bmatrix}\phi_i & 0 & 0 & 0 & 0\\ 0 & \phi_i & 0 & 0 & 0\\ 0 & 0 & \phi_i & 0 & 0\\ 0 & 0 & 0 & \phi_i & 0\\ 0 & 0 & 0 & 0 & \phi_i\end{bmatrix},\overline{\mathbf{M}}=\begin{bmatrix}I_0 & 0 & 0 & I_1 & 0\\ 0 & I_0 & 0 & 0 & I_1\\ 0 & 0 & I_0 & 0 & 0\\ I_1 & 0 & 0 & I_2 & 0\\ 0 & I_1 & 0 & 0 & I_2\end{bmatrix} \quad (19)$$

where I_0, I_1, and I_2 are the normal, coupled normal-rotary, and rotary inertial coefficients, respectively. These coefficients are defined by

$$(I_0,I_1,I_2)=\int_{-h/2}^{h/2}\rho(z)(1,z,z^2)dz \quad (20)$$

The arrays of bending-extensional coupling stiffness matrix $\overline{\mathbf{B}}$ are zero for symmetric laminated composites.

Finally, through a derivative with respect to displacement vector $\hat{\mathbf{d}}$, Eq. (17) can be expressed as

$$\mathbf{M}\ddot{\hat{\mathbf{d}}}+\mathbf{K}\hat{\mathbf{d}}=\mathbf{F} \quad (21)$$

in which $\mathbf{M}$, $\mathbf{K}$, and $\mathbf{F}$ are the mass matrix, stiffness matrix, and force vector, respectively. These are defined as

$$\mathbf{M}=\int_A\mathbf{G}_i^T\overline{\mathbf{M}}\mathbf{G}_j dA \quad (22)$$
$$\mathbf{K}=\mathbf{K}_m+\mathbf{K}_b+\mathbf{K}_s+\mathbf{K}_w+\mathbf{K}_p \quad (23)$$
$$\mathbf{F}=\int_A\boldsymbol{\varphi}_w^Tq(t)dA \quad (24)$$

where $\mathbf{K}_m$, $\mathbf{K}_b$, and $\mathbf{K}_s$ are the stiffness matrixes of extensional, bending-extensional, and bending modes, respectively. $\mathbf{K}_w$ and $\mathbf{K}_p$ are the stiffness matrixes that represent Winkler and Pasternak elastic foundations. They are defined in the following equations:

$$\mathbf{K}_m=\int_A\left[\mathbf{B}_m^T\mathbf{A}\mathbf{B}_m+\mathbf{B}_m^T\overline{\mathbf{B}}\mathbf{B}_b+\mathbf{B}_b^T\overline{\mathbf{B}}\mathbf{B}_m\right]dA,$$
$$\mathbf{K}_b=\int_A\mathbf{B}_b^T\mathbf{D}\mathbf{B}_b dA\ ,\ \mathbf{K}_s=\int_z\mathbf{B}_s^T\mathbf{A}_s\mathbf{B}_s dA \quad (25)$$

$$\mathbf{K}_w=\int_A\boldsymbol{\varphi}_w^Tk_w\boldsymbol{\varphi}_w dA\ ,\ \mathbf{K}_p=\int_A\mathbf{B}_p^Tk_s\mathbf{B}_p dA \quad (26)$$

For numerical integration, the problem domain is discretized to a set of background cells with Gauss points inside each cell. Then, global stiffness matrix $\mathbf{K}$ is obtained numerically by sweeping all the Gauss points.

The imposition of essential boundary conditions in the system of Eq. (21) is impossible because moving least squares shape functions do not satisfy the Kronecker delta property. As previously stated, this work uses a transfer function method in implementing essential boundary conditions. For this purpose, a transformation matrix is constructed by establishing a relationship between nodal displacement vector $\mathbf{d}$ and virtual displacement vector $\hat{\mathbf{d}}$.

$$\mathbf{d}=\mathbf{T}\hat{\mathbf{d}} \quad (27)$$

$\mathbf{T}$ is the transformation matrix that is a $5N\times5N$ matrix. For each node, this matrix is defined as

$$\mathbf{T}=\begin{bmatrix}\phi_1(x_1)\times\mathbf{I}_{(5\times5)} & \phi_1(x_2)\times\mathbf{I}_{(5\times5)} & \cdots & \phi_1(x_N)\times\mathbf{I}_{(5\times5)}\\ \phi_2(x_1)\times\mathbf{I}_{(5\times5)} & \phi_2(x_2)\times\mathbf{I}_{(5\times5)} & \cdots & \phi_2(x_N)\times\mathbf{I}_{(5\times5)}\\ \vdots & \vdots & \cdots & \vdots\\ \phi_N(x_1)\times\mathbf{I}_{(5\times5)} & \phi_N(x_2)\times\mathbf{I}_{(5\times5)} & \cdots & \phi_N(x_N)\times\mathbf{I}_{(5\times5)}\end{bmatrix} \quad (28)$$

where $\mathbf{I}_{(5\times5)}$ is an identity matrix of size 5. Using Eq. (27) rearranges the system of linear Eq. (21) to

$$\hat{\mathbf{M}}\ddot{\mathbf{d}}+\hat{\mathbf{K}}\mathbf{d}=\hat{\mathbf{F}} \quad (29)$$

where

$$\hat{\mathbf{M}}=\mathbf{T}^{-T}\mathbf{M}\mathbf{T}^{-1}\ ,\ \hat{\mathbf{K}}=\mathbf{T}^{-T}\mathbf{K}\mathbf{T}^{-1}\ ,\ \hat{\mathbf{F}}=\mathbf{T}^{-T}\mathbf{F} \quad (30)$$

Now, the essential B. Cs. can be easily enforced in the modified system of Eq. (29), as is possible with the finite element method. In this work, the Newmark (central difference) method is used for the solution of Eq. (29) in the time domain.

In this method, the displacement field is obtained in each time step as follows:

$$\ddot{\mathbf{d}}^t = \hat{\mathbf{M}}^{-1}\left[\hat{\mathbf{F}}^t - \hat{\mathbf{K}}\mathbf{d}^t\right] \quad (31)$$

$$\mathbf{d}^{t+dt} = dt^2\ddot{\mathbf{d}}^t + 2\mathbf{d}^t - \mathbf{d}^{t-dt} \quad (32)$$

where t shows the times, and dt is the size of a time step.

By solving Eq. (29), the time history of the displacement field and then stress wave propagation can be derived with the consideration of type of periodic or impact loading. In the absence of external forces, Eq. (29) is simplified in this manner:

$$\hat{\mathbf{M}}\ddot{\mathbf{d}} + \hat{\mathbf{K}}\mathbf{d} = 0 \quad (33)$$

Thus, the natural frequencies and mode shapes of the plates are determined by solving this eigenvalue problem.

5. RESULTS AND DISCUSSION

This section discusses numerical examples of the free vibration, forced vibration, resonance, and stress wave propagation behaviors of the examined orthotropic FGM sandwich plates. As mentioned earlier, the plates are subjected to periodic or impact loading, and the developed mesh-free approach and the Newmark method are used. The frequencies of the sandwich plates are derived and investigated through the consideration of their resonance behaviors.

First, the convergence and accuracy of the mesh-free method in determining the vibrational behaviors of the plates are examined by a comparison between the results and those reported in the literature. Second, the mesh-free results on the vibrational and dynamic characteristics of the plates are presented.

In simulations, the orthotropic FGM sandwich plates are assumed to be made of a homogeneous glass-epoxy core and two FGM face sheets. In the face sheets, the material volume fractions are varied from those of the glass-epoxy at the interfaces of the core and from those of the graphite-epoxy at the faces of the sandwich plates. The modifications are conducted using Eq. (1) (Fig. 2). The material properties of the glass-epoxy and graphite-epoxy are listed in Table 1. Note that transverse isotropic materials are a special class of orthotropic materials that have the same properties in one plane (e.g., the x-y plane) and different properties in the direction normal to the aforementioned plane (e.g., the z-axis). Thus, glass-epoxy and graphite-epoxy are transverse isotropic materials. In all the examples of the orthotropic sandwich plates, the foundational parameters are presented in the non-dimensional forms $K_w=k_wa^4/D$ and $K_s=k_sa^2/D$, in which $D=E_1h^3/12(1-\upsilon_{12}^2)$ is a reference bending rigidity of the plate and is based on the mechanical properties of graphite-epoxy. The non-dimensional deflections (for forced and dynamic analyses) and natural frequencies of the orthotropic sandwich plates are based on the mechanical properties of graphite-epoxy and glass-epoxy, respectively. The deflection and frequency are defined as [13]

$$\overline{w} = 10E_1h^3w/q_0a^4 \quad (34)$$

$$\hat{\omega} = \omega h\sqrt{\rho/E_1} \quad (35)$$

where q_0 is the value of the amplitude of time-dependent applied load, and w denotes the central deflection of the plates. The following sets of support conditions are employed to compute the desired responses:

(a) Simply supported conditions

at x=0 and a: $v=w=\theta_y=0$ and at y=0 and b: $u=w=\theta_x=0$

(b) Clamped conditions:

at x=0 and a: and at y=0 and b: $u=v=w=\theta_x=\theta_y=0$

Table 1 Material properties of the examined orthotropic (transverse isotropic) materials [53]

Materials	E_1 (GPa)	E_2 (GPa)	E_3 (GPa)	υ_{23}	υ_{31}	υ_{12}	G_{23} (GPa)	G_{31} (GPa)	G_{12} (GPa)	ρ (kg/m^3)
Graphite-epoxy	155	12.1	12.1	0.458	0.248	0.248	3.2	4.4	4.4	1500
Glass-epoxy	50	15.2	15.2	0.428	0.254	0.254	3.28	4.7	4.7	1800

5.1 Validation of models

To investigate the convergence and accuracy of the developed method, let us consider a simply supported FGM square plate, as was done by Thai and Choi [21]. Fig. 3 depicts the convergence of the proposed mesh-free method in the non-dimensional fundamental frequencies of the plates resting on Winkler-Pasternak elastic foundations at h/a=0.2, K_w=100 and K_s=100, and volume fraction exponents of n=0 and n=1. These values reveal that using only a 5×5 node arrangement enables the proposed method to achieve very good accuracy and agreement with the results of Thai and Choi [21] for the homogeneous (n=0) and FGM (n=1) plates. The non-dimensional fundamental frequencies of these plates are presented in Table 2 for various values of h/a (0.05, 0.1, and 0.2) and elastic foundation coefficients. The table shows that the proposed method exhibits very good accuracy and agreement with previously reported results, especially with respect to thin plates.

5.2 Free vibration of orthotropic FGM sandwich plates

Clamped orthotropic FGM sandwich plates are examined to investigate the effects of material dis-

tributions, elastic foundation coefficients, and geometric dimensions on the natural frequencies of the plates. Table 3 lists the non-dimensional fundamental frequencies of the plates at different elastic foundation coefficients (K_w and K_s), aspect ratios (b/a=1 and 3), plate thickness ratios (h/a=0.1 and 0.2), face sheet thickness ratios (h_f/h=0.1 and 0.2), and volume fraction exponents (n=0, 0.1, 1, 10, and 100). The frequency parameter decreases with an increase in b/a from 1 to 3 because the plate manners are near the beam manners. An increase in h/a and h_f/h and a decrease in volume fraction exponent increase the frequency parameter. The values of h/a significantly affect the frequency parameter of orthotropic FGM sandwich plates. Finally, the elastic foundation also increases the frequency parameter.

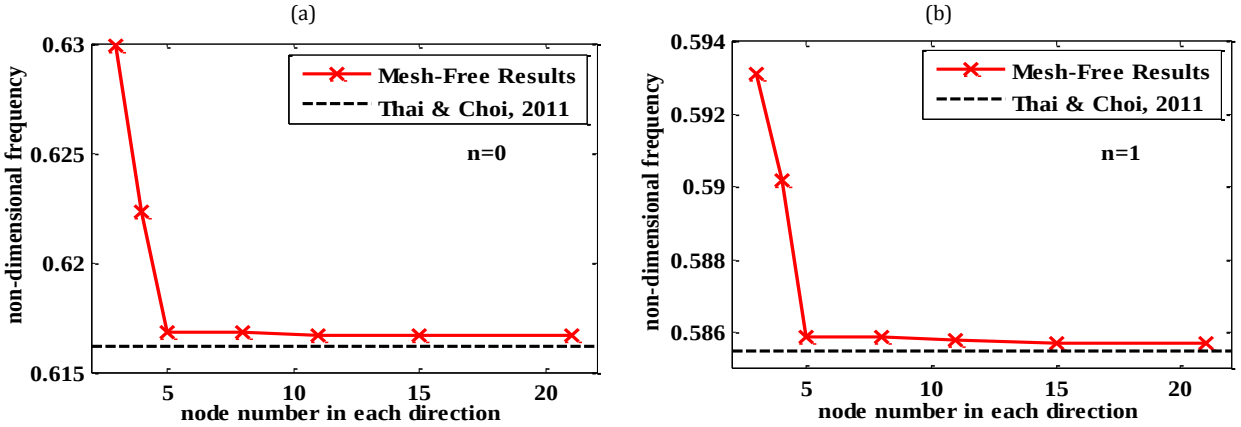

Figure 3 Convergence of non-dimensional fundamental frequency ($\hat{\omega}$) of the FGM plate at (a) n=0; (b) n=1 and h/a=0.2, K_w=100, K_s=100 for different numbers of nodes in each direction

Table 2 Comparison of normalized fundamental frequencies, $\hat{\omega}$, in simply supported square FGM plates

K_w	K_s	h/a	Method	n=0	n=1
0	0	0.05	Present	0.0291	0.0222
			[54]	0.0291	0.0227
			[21]	0.0291	0.0222
		0.1	Present	0.1135	0.0869
			[54]	0.1134	0.0891
			[21]	0.1135	0.0869
		0.2	Present	0.4167	0.3216
			[54]	0.4154	0.3299
			[21]	0.4154	0.3207
100	100	0.05	Present	0.0411	0.0384
			[54]	0.0411	0.0388
			[21]	0.0411	0.0384
		0.1	Present	0.1618	0.1519
			[54]	0.1619	0.1542
			[21]	0.1619	0.1520
		0.2	Present	0.6167	0.5857
			[54]	0.6162	0.5978
			[21]	0.6162	0.5855

Table 3 Non-dimensional fundamental frequencies, $\hat{\omega}$, in clamped orthotropic FGM sandwich plates

b/a	h/a	h_f/h	K_w	K_s	n				
					0	0.1	1	10	100
1	0.1	0.1	0	0	0.0758	0.0753	0.0724 *	0.0681	0.0668
			100	10	0.1203	0.1199	0.1177 **	0.1146	0.1138
		0.2	0	0	0.0797	0.0791	0.0757	0.0693	0.0670
			100	10	0.1240	0.1234	0.1203	0.1154	0.1139
	0.2	0.1	0	0	0.1983	0.1978	0.1947	0.1896	0.1880
			100	10	0.4177	0.4169	0.4132	0.4086	0.4073
		0.2	0	0	0.2026	0.2020	0.1982	0.1911	0.1882
			100	10	0.4255	0.4241	0.4177	0.4098	0.4075
3	0.1	0.1	0	0	0.0661	0.0655	0.0617	0.0561	0.0544
			100	10	0.1023	0.1018	0.0991	0.0955	0.0944
		0.2	0	0	0.0710	0.0702	0.0658	0.0596	0.0546
			100	10	0.1064	0.1057	0.1021	0.0964	0.0946

* 2nd frequency: 0.1090, 3rd frequency: 0.1430
** 2nd frequency: 0.1693, 3rd frequency: 0.1927

5.3 Forced vibration of orthotropic FGM sandwich plates

Square orthotropic FGM sandwich plates are subjected to periodic uniform pressure loading at the top face of the sandwich plates as follows:

$$P(t) = q_0 \sin(\omega_t t) \tag{36}$$

where ω_t is the frequency of time-dependent applied load and is equal to $\omega_0 = 2500\, rad/s$ in the succeeding simulation.

The effects of loading frequency on the time history of the central deflection of the orthotropic FGM sandwich plates are investigated. Let us consider clamped square plates with h/a=0.1, h_f/h=0.1, and n=1 and subjected to time-dependent pressure at loading frequencies of ω_0, $\omega_0/2$, and $\omega_0/4$. Figs. 4a and 4b show the time histories of the normalized central deflections of the plates without an elastic foundation and with resting on the Pasternak foundation (K_w=100 and K_s=10), respectively. The figures indicate that the severity of the elastic foundation decreases the central deflections of the sandwich plates and that the amplitudes of the deflections are reduced by a decrease in loading frequency.

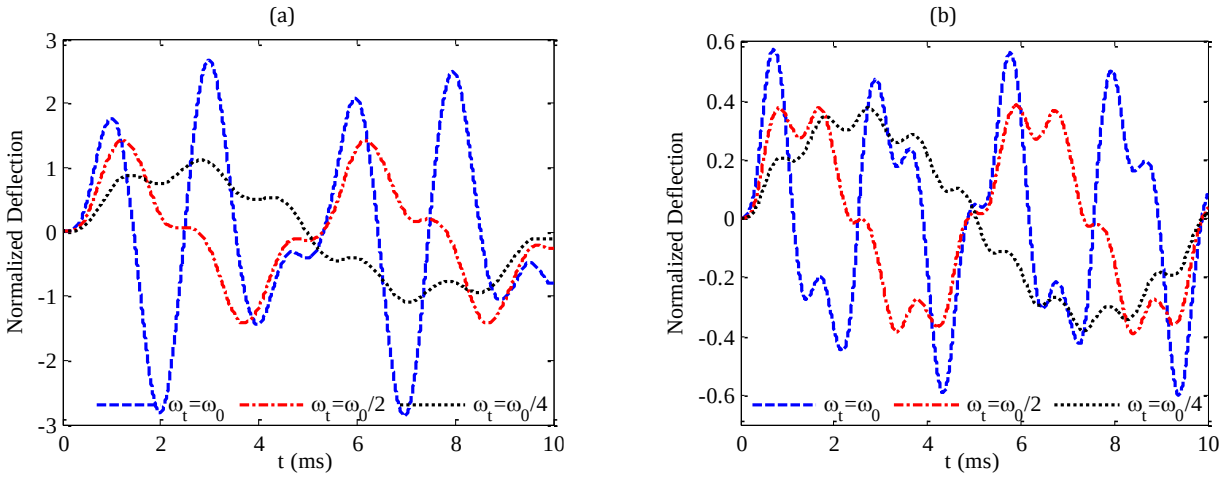

Figure 4 Time history of normalized central deflections ($\overline{w}$) of clamped orthotropic FGM sandwich plates at (a) K_w=0, K_s=0; (b) K_w=100, K_s=10, and b/a=1, h/a=0.1, h_f/h=0.1, and n=1

Now, let us consider square clamped sandwich plates subjected to periodic pressure ($\omega_t = \omega_0$) and resting on the elastic foundation (K_w=100 and K_s=10) to delve into the effects of the plates' geometric dimensions on the time history of deflection. Fig. 5 illustrates the time history of the plates' normalized central deflections at h/a=0.1 and 0.2, h_f/h=0.1 and 0.2, and n=0, 0.1, 1, and 10. The amplitudes of the deflections decline with decreasing volume fraction exponent. Such amplitudes also decrease with increasing h/a and h_f/h. The thickness of the plates (h/a) is higher than that of the face sheets (h_f/h).

Finally, the effects of essential boundary conditions on the forced vibration behaviors of orthotropic FGM sandwich plates subjected to a periodic load of $\omega_t = \omega_0$ are investigated. Fig. 6 show the time history of the normalized central deflections of the plates at h/a=0.1, h_f/h=0.1, K_w=100 and K_s=10, and n=0, 0.1, 1, and 10 for the boundary conditions of CSCS and CFCF, where C, S, and F denote clamped, simply supported, and free edges, respectively. Comparing Figs. 6 and 5a indicates that the clamped and CFCF sandwich plates have the smallest and largest deflection amplitudes, respectively.

5.4 Resonance behavior of orthotropic FGM sandwich plates

The resonance of orthotropic FGM sandwich plates are also explored. Let us consider sandwich plates subjected to periodic uniform loading at the top face of the sandwich plates, as with Eq. (36), in which loading frequency ω_t is equal to the n^{th} natural frequency ω_n of the sandwich plates reported in Table 3.

Figs. 7a and 7b illustrate the time histories of the normalized central deflections of these sandwich plates without an elastic foundation and with resting on the Pasternak foundation (K_w=100 and K_s=10), respectively. These sandwich plates are clamped at h/a=0.1, h_f/h=0.1, and n=1 and subjected to periodic loading with loading frequencies equal to the first, second, and third frequencies of the sandwich plates (i.e., $\omega_t = \omega_1, \omega_2, \omega_3$). This loading leads to a divergence in the amplitudes of deflection in the first mode despite the elastic foundation's reduction of deflection amplitudes.

Fig. 8 presents the first mode of resonance in the clamped orthotropic sandwich plates at b/a=1, h/a=0.1 and 0.2, h_f/h=0.1 and 0.2, and n=0, 0.1, 1, and 10. An increase in h/a elevates the amplitudes of deflection and decreases the periods of their vibration because of the increase in frequency loading. The volume fraction exponent exerts a stronger effect on the periods of vibrations through an increase in h_f/h.

5.5 Dynamic behavior of orthotropic FGM sandwich plates

Now, the dynamic behaviors of orthotropic FGM sandwich plates resting on an elastic foundation are determined by considering sandwich plates subjected to an impact uniform pressure load at the top face of the plates as follows:

$$\begin{aligned} &P(t)=q_0 \sin 4000\pi t \quad \text{for } t \le 0.25 \text{ (ms)} \\ &P(t)=0 \qquad\qquad\quad \text{for } t > 0.25 \text{ (ms)} \end{aligned} \tag{35}$$

Let us consider clamped orthotropic FGM sandwich plates subjected to an impact load, as with Eq. (37), and resting on the Pasternak elastic foundation at b/a=1, h/a=0.1, h_f/h=0.1, K_w=100, and K_s=10 (a=1 m, q_0=0.1 MPa). Fig. 9 shows the time history of stress wave propagation (σ_{xx}, σ_{yy}, σ_{xy}, σ_{xz}, and σ_{yz}) at the top face and central deflection of the sandwich plates for n=0.1, 1, and 10. The amplitudes of normal stresses are higher than those of shear stresses. An increasing volume fraction exponent

leads to a rise in the amplitudes of stresses and a decline in wave speed. After load is eliminated, the sandwich plates show harmonic vibration with amplitudes less than those of the same forced vibration (in Fig. 5a).

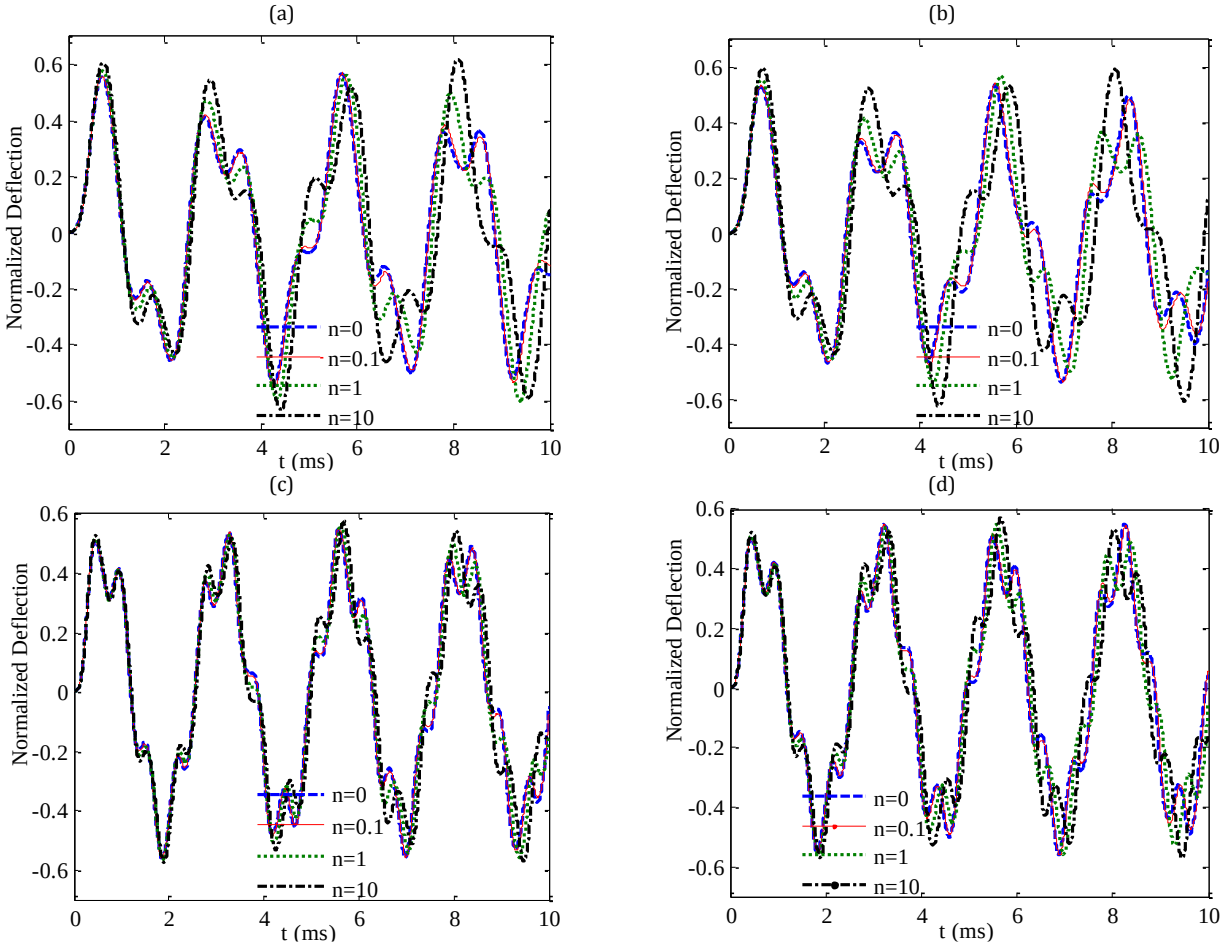

Figure 5 Time history of normalized central deflections ($\overline{w}$) of clamped orthotropic FGM sandwich plates at (a) h/a=0.1, h_f/h=0.1; (b) h/a=0.1, h_f/h=0.2; (c) h/a=0.2, h_f/h=0.1; (d) h/a=0.1, h_f/h=0.1, and b/a=1, K_w=100, K_s=10, and $\omega_t = \omega_0$

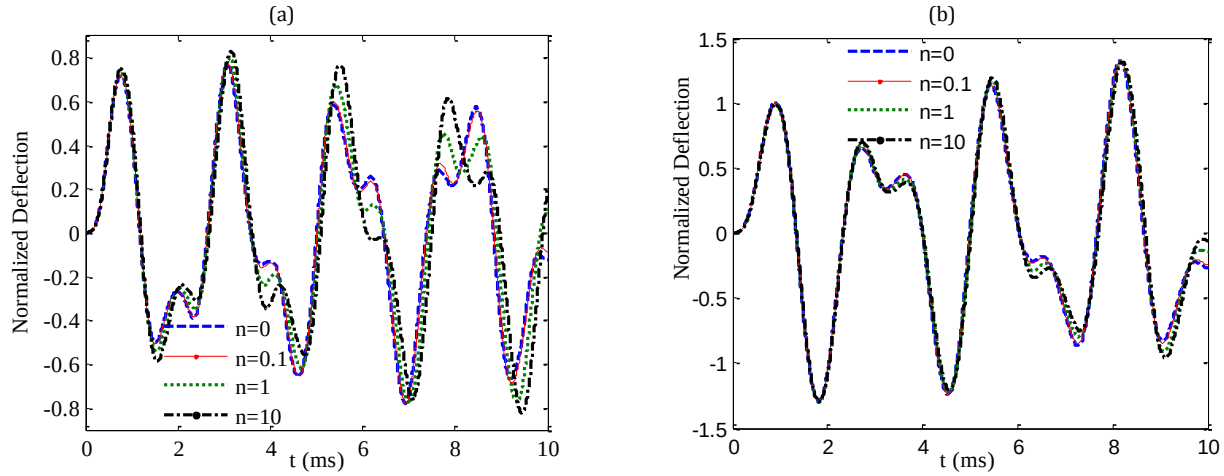

Figure 6 Time history of normalized central deflections ($\overline{w}$) of (a) CSCS, (b) CFCF orthotropic FGM sandwich plates at b/a=1, h/a=0.1, h_f/h=0.1, K_w=100, K_s=10, and $\omega_t = \omega_0$

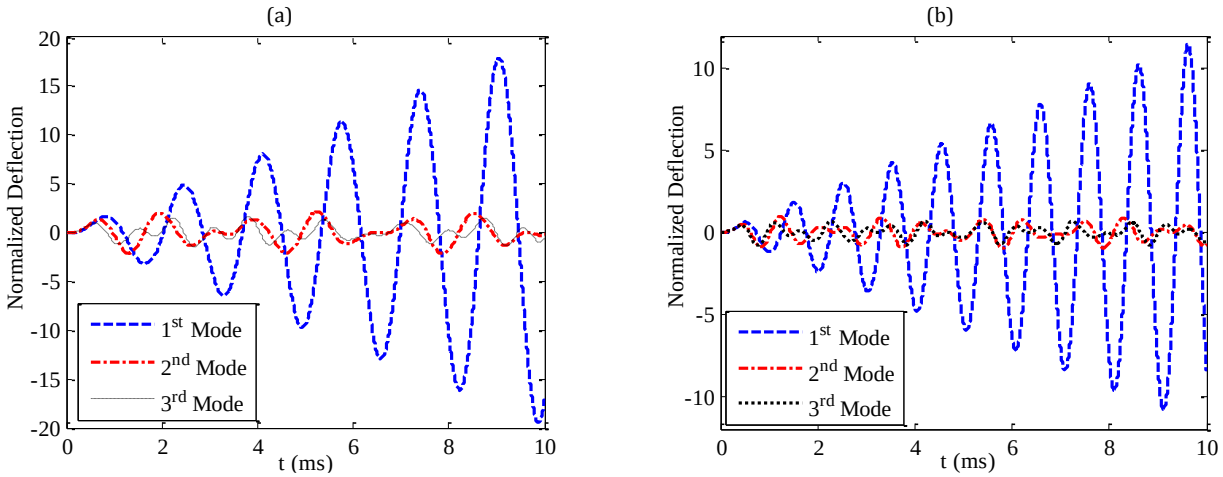

Figure 7 Time history of normalized central deflections ($\overline{w}$) of orthotropic FGM sandwich plates at (a) K_w=0, K_s=0; (b) K_w=100, K_s=10, and b/a=1, h/a=0.1, h_f/h=0.1, and n=1

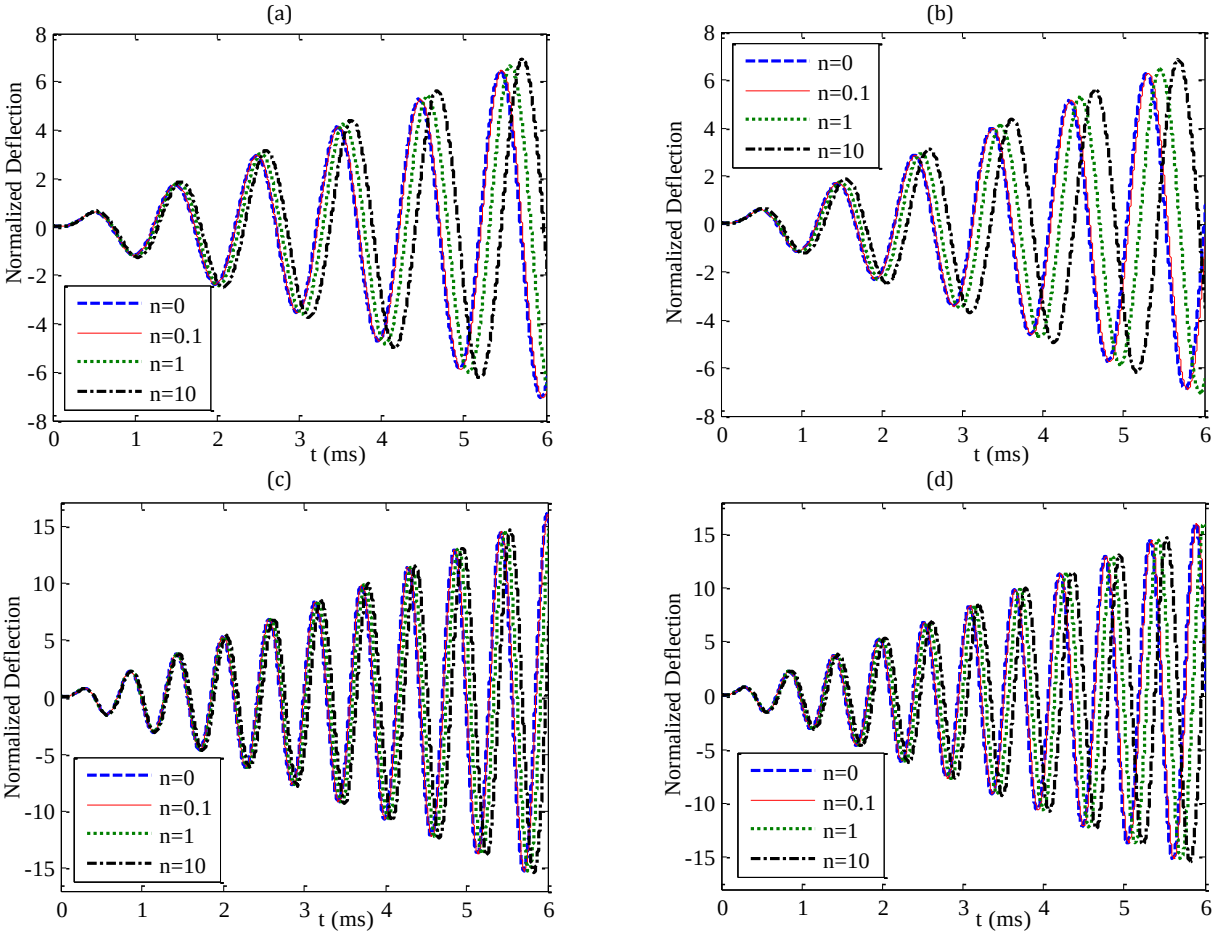

Figure 8 Time history of normalized central deflections ($\overline{w}$) of clamped orthotropic FGM sandwich plates at (a) h/a=0.1, h_f/h=0.1; (b) h/a=0.1, h_f/h=0.2; (c) h/a=0.2, h_f/h=0.1; (d) h/a=0.1, h_f/h=0.1, and b/a=1, K_w=100, K_s=10, and $\omega_t = \omega_0$

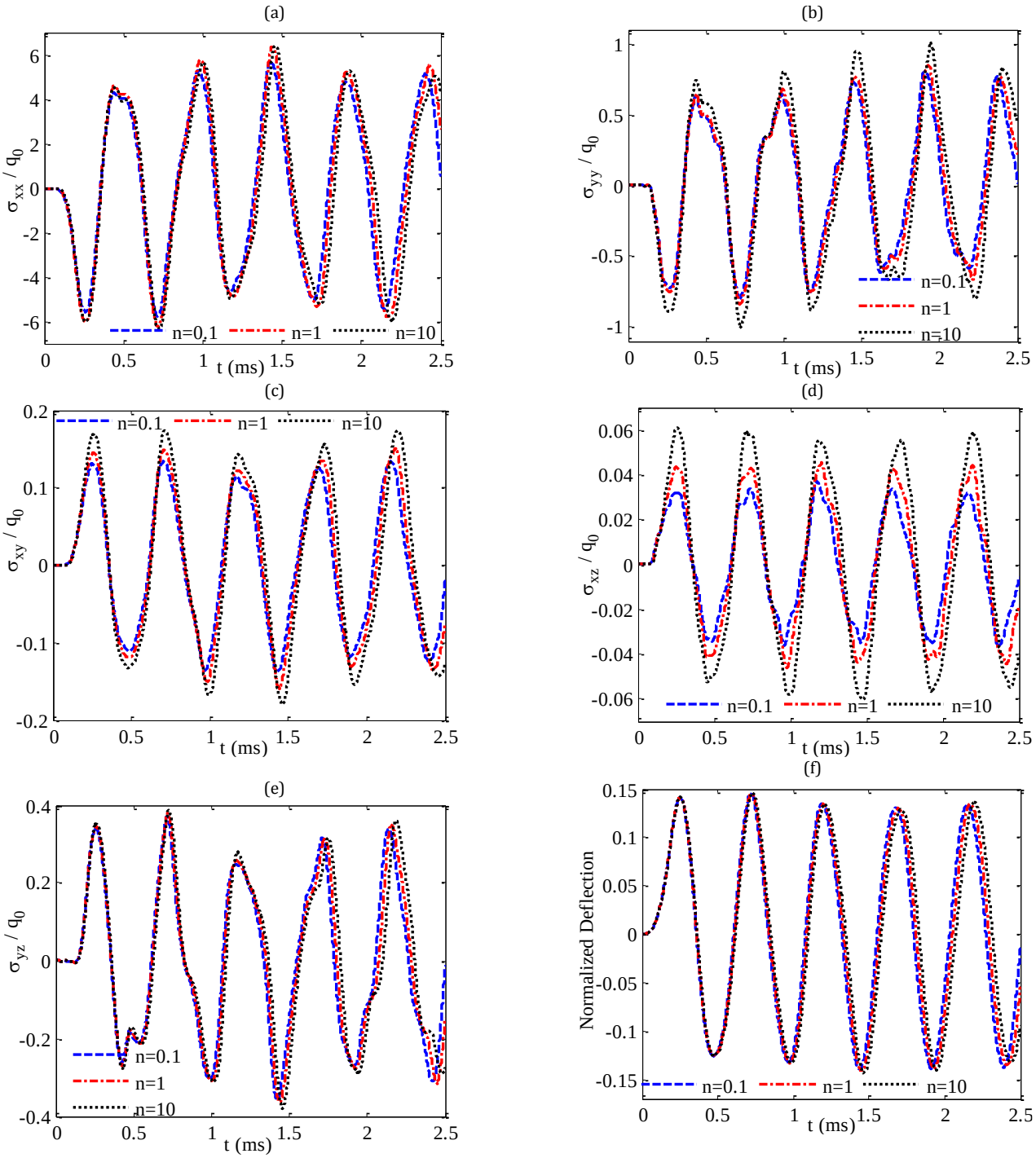

Figure 9 Time history of (a) σ_{xx}, (b) σ_{yy}, (c) σ_{xy}, (d) σ_{xz}, (e) σ_{yz}, and (f) $\overline{w}$ at the top face of clamped orthotropic FGM sandwich plates at b/a=1, h/a=0.1, h_f/h=0.1, K_w=100, and K_s=10

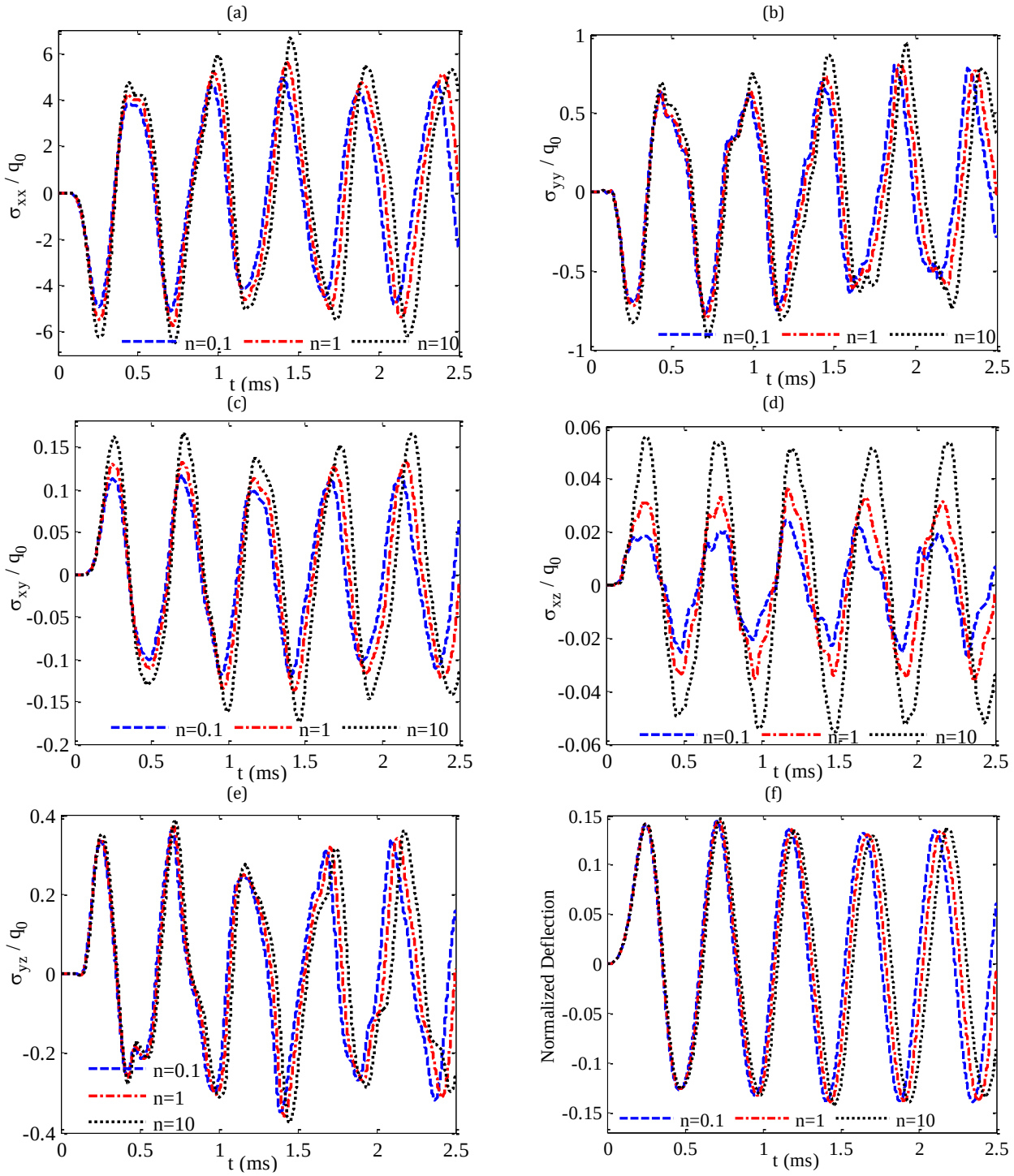

Figure 10 Time history of (a) σ_{xx}, (b) σ_{yy}, (c) σ_{xy}, (d) σ_{xz}, (e) σ_{yz}, and (f) $\overline{w}$ at the top face of clamped orthotropic FGM sandwich plates at b/a=1, h/a=0.1, h_f/h=0.2, K_w=100, and K_s=10

Let us consider the same sandwich plates but with h_f/h=0.2 as the variable. Fig. 10 displays the stress wave propagation and central vibration of the plates. The comparison of Figs. 10 and 9 indicates that the plates exhibit almost the same dynamic behaviors but that the volume fraction exponent exerts a stronger effect on the plates with thicker face sheets.

Finally, let us re-examine the first model of dynamic analysis but with h/a=0.2 as the variable. The time history of stress wave propagation and the central vibration of the orthotropic FGM sandwich plates are illustrated in Fig. 11. The comparison of Figs. 9 and 11 demonstrates that an increase in the thickness of the sandwich plates leads to a decrease in the amplitudes of stresses and vibrations and the

speeds of wave propagation. Fig. 12 shows the time history of the normal stresses of the sandwich plate with n=10 imposed at the top, middle, and bottom planes (z=−h, 0, h). The sandwich plate at z=0 senses almost no normal stresses, whereas the top and bottom planes sense the same in-plane stresses but with a different sign.

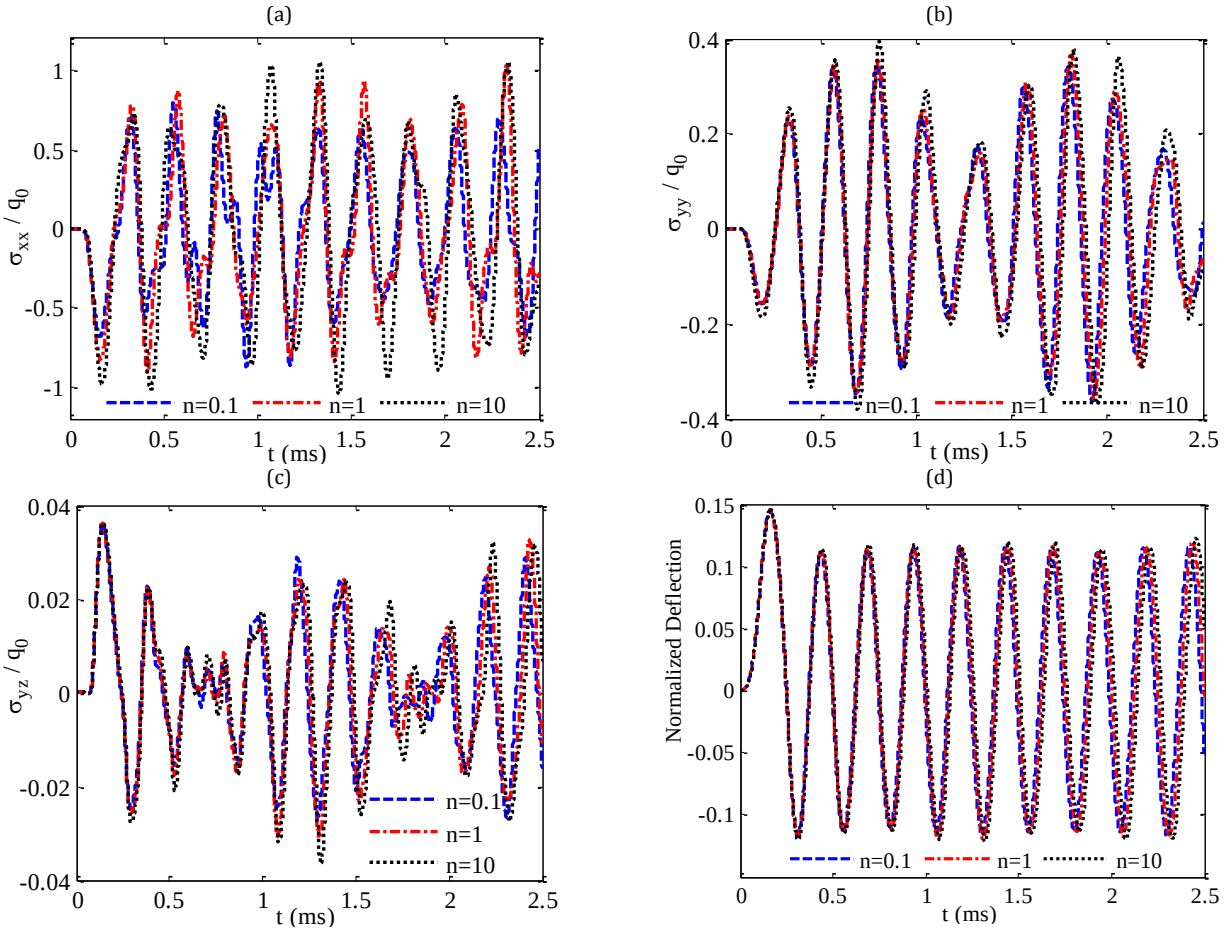

Figure 11 Time history of (a) σ_{xx}, (b) σ_{yy}, (c) σ_{yz}, and (d) $\overline{w}$ at the top face of clamped orthotropic FGM sandwich plates at b/a=1, h/a=0.2, h_f/h=0.1, K_w=100, and K_s=10

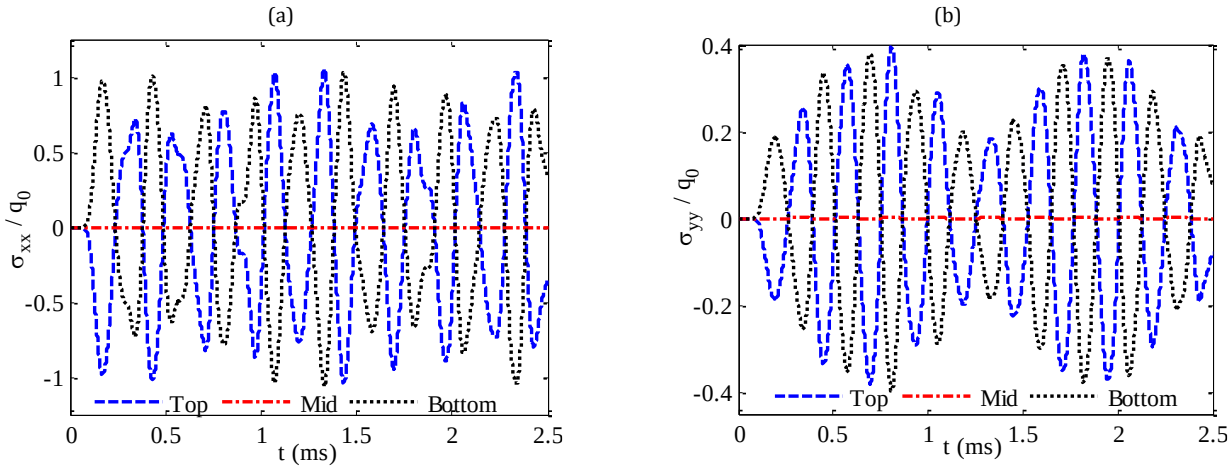

Figure 12 Time history of (a) σ_{xx} and (b) σ_{yy} at the top, middle, and bottom planes of clamped orthotropic FGM sandwich plates at n=10, b/a=1, h/a=0.1, h_f/h=0.2, K_w=100, and K_s=10

6. CONCLUSION

In this study, the vibration, resonance, and dynamic behaviors of orthotropic FGM sandwich plates resting on a Pasternak elastic foundation are analyzed using a developed mesh-free method based on FSDT and moving least squares shape functions. Essential boundary conditions are imposed via a transfer function method. The sandwich plates are assumed to be composed of a homogeneous orthotropic core and two orthotropic FGM face sheets made of two orthotropic materials. Numerical examples are provided to illuminate the vibrational and dynamic characteristics of the plates at different elastic foundation coefficients, material distributions, geometrical dimensions, time-depended loading levels, and boundary conditions. The primary findings are summarized as follows:

- The mesh-free method exhibits good convergence and accuracy in the vibrational analysis of the orthotropic FGM plates.
- Increasing sandwich plate thickness and face sheet thickness increase the frequency parameter.
- The severity of the elastic foundation decreases the vibration amplitudes of the sandwich plates.
- Decreasing loading frequency reduces the vibration amplitudes.
- Loading with fundamental frequency leads to a divergence in vibration amplitudes (resonance phenomenon).
- After load elimination, the sandwich plates show harmonic vibration with amplitudes less than those of the same forced vibration.
- The amplitudes of normal stresses are higher than those of shear stresses.
- An increase in volume fraction exponent leads to a rise in the amplitudes of stresses and a decline in wave speed.
- Plate thickness h/a exerts a stronger effect on the vibrational and dynamic behaviors of the sandwich plates than does the thickness of face sheets h_f/h.
- The sandwich plate at z=0 senses almost no in-plane stresses, whereas the top and bottom planes sense the same in-plane stresses but with a different sign.
- An increase in the thickness of the sandwich plates leads to a decrease in the amplitudes of stresses and vibrations and the speeds of wave propagation.

References

[1] Koizumi M. The concept of FGM. *Ceram Trans Func Grad Mater* 1993; 34: 3–10.

[2] Winkler E. 1867, Die Lehre von der Elasticitaet und Festigkeit, Dominicus, Prag.

[3] Pasternak PL. 1954, On a new method of analysis of an elastic foundation by means of two foundation constants (in Russian), Gosudarstrennoe Izdatelstvo Literaturi po Stroitelstvu i Arkhitekture, Moscow, USSR.

[4] Reddy JN. 2004, Mechanics of Laminated Composite Plates and Shells: Theory and Analysis, CRC.

[5] Reissner E. The effect of transverse shear deformation on the bending of elastic plates, *J Applied Mech,* 1945; 12: 69–72.

[6] Mindlin RD. Influence of rotatory inertia and shear on flexural motions of isotropic, elastic plates, *J Applied Mech,* 1951; 18: 31–38.

[7] Thai HT, Choi DH. An efficient and simple refined theory for buckling analysis of functionally graded plates. *Applied Math Modelling,* 2012; 36: 1008–1022.

[8] Reddy JN. A simple higher order theory for laminated composite plates. *J Applied Mech,* 1984; 51: 745-752.

[9] Kundalwal, SI, Kumar, RS, Ray, MC, Smart damping of laminated fuzzy fiber reinforced composite shells using 1–3 piezoelectric composites, *Smart Mater Struct*, 2013: 22, 105001.

[10] Kundalwal, SI, Meguid, SA, Effect of carbon nanotube waviness on active damping of laminated hybrid composite shells, *Acta Mech*, 2015; 226, 2035–2052.

[11] Kundalwal, SI, Ray MC, Smart damping of fuzzy fiber reinforced composite plates using 1--3 piezoelectric composites, *J Vib Control*, 2016; 22: 1526-1546.

[12] Aiello MA, Ombres L. Buckling Load Design of Sandwich Panels Made with Hybrid Laminated Faces and Transversely Flexible Core. *J Sandwich Struct Mater,* 2007; 9: 467-485.

[13] Ferreira AJM, Castro LMS, Bertoluzza S. A high order collocation method for the static and vibration analysis of composite plates using a first-order theory. *Compos Struct,* 2009; 89: 424–432.

[14] Ferreira AJM, Roque CMC, Martins PALS. Analysis of composite plates using higher-order shear deformation theory and a finite point formulation based on the multiquadric radial basis function method. *Composites Part B* 2003; 34: 627–36.

[15] Shariyat M. Dynamic buckling of imperfect laminated plates with piezoelectric sensors and actuators subjected to thermo-electro-mechanical loadings, considering the temperature-dependency of the material properties. *Compos Struct,* 2009; 88: 228–239.

[16] Huang XL, Shen HS. Vibration and dynamic response of functionally graded plates with pie-

zoelectric actuators in thermal environments. *J Sound Vibr,* 2006; 289: 25–53.

[17] Xia XK, Shen HS. Nonlinear vibration and dynamic response of FGM plates with piezoelectric fiber reinforced composite actuators, *Compos Struct,* 2009; 90: 254–262.

[18] Malekzadeh P, Golbahar Haghighi MR, Gholami M, Dynamic response of thick laminated annular sector plates subjected to moving load, *Compos Struct,* 2010; 92: 155–163.

[19] Zhang W, Yang J, Hao Y. Chaotic vibrations of an orthotropic FGM rectangular plate based on third-order shear deformation theory, *Nonlinear Dyn,* 2010; 59: 619–660

[20] Dehghan M, BaradaranGH. Buckling and free vibration analysis of thick rectangular plates resting on elastic foundation using mixed finite element and differential quadrature method, *Applied Math Comput,* 2011; 218: 2772–2784.

[21] Thai HT, Choi DH. A refined plate theory for functionally graded plates resting on elastic foundation, *Compos Sci Technol,* 2011; 71: 1850–1858.

[22] Thai HT, Choi DH. An efficient and simple refined theory for buckling analysis of functionally graded plates, *Applied Math Modelling,* 2012; 36: 1008–1022.

[23] Asemi K, Shariyat M. Highly accurate nonlinear three-dimensional finite element elasticity approach for biaxial buckling of rectangular anisotropic FGM plates with general orthotropy directions, *Compos Struct,* 2013; 106: 235-249.

[24] Mansouri MH, Shariyat M. Biaxial thermo-mechanical buckling of orthotropic auxetic FGM plates with temperature and moisture dependent material properties on elastic foundations, *Composites Part B* 2015; 83: 88-104.

[25] Shariyat M, Asemi K. Three-dimensional nonlinear elasticity-based 3D cubic B-spline finite element shear buckling analysis of rectangular orthotropic FGM plates surrounded by elastic foundations, *Composites Part B* 2014; 56: 934-947.

[26] Sofiyev AH, Huseynov SE, Ozyigit P, Isayev FG. The effect of mixed boundary conditions on the stability behavior of heterogeneous orthotropic truncated conical shells, *Meccanica* 2015; 50: 2153-2166.

[27] Tahouneh, V, Eskandari-Jam, J, A Semi-analytical Solution for 3-D Dynamic Analysis of Thick Continuously Graded Carbon Nanotube-reinforced Annular Plates Resting on a Two-parameter Elastic Foundation, *Mech Adv compos struct*, 2014; 1, 113-130.

[28] Tahouneh, V, Naei, MH, Semi-Analytical Solution for Free Vibration Analysis of Thick Laminated Curved Panels with Power-Law Distribution FG Layers and Finite Length Via Two-Dimensional GDQ Method, *J solid mech*, 2016; 8, 334-347.

[29] Tahouneh, V, Naei, MH, The effect of multi-directional nanocomposite materials on the vibrational response of thick shell panels with finite length and rested on two-parameter elastic foundations, *Int J Adv Struct Eng*, 2016; 8, 11-28.

[30] Tahouneh, V, Using an equivalent continuum model for 3D dynamic analysis of nanocomposite plates, *Steel Compos Struct*, 2016; 20, 623-649.

[31] Tahouneh, V, Naei, MH, Free vibration and vibrational displacements analysis of thick elastically supported laminated curved panels with power-law distribution functionally graded layers and finite length via 2D GDQ method, *J Sand Struct Mater*, 2016; 18, 263-293.

[32] Tahouneh, V, Naei, MH, Using Eshelby-Mori-Tanaka scheme for 3D free vibration analysis of sandwich curved panels with functionally graded nanocomposite face sheets and finite length, *Polym Compos*, 2016; DOI: 10.1002/pc. 23929.

[33] Tahouneh, V, Yas, MH, Tourang, H, Kabirian, M, Semi-analytical solution for three-dimensional vibration of thick continuous grading fiber reinforced (CGFR) annular plates on Pasternak elastic foundations with arbitrary boundary conditions on their circular edges, *Meccanica*, 2013; 48, 1313-1336.

[34] Tahouneh, V, Yas, MH, Influence of equivalent continuum model based on the Eshelby-Mori-Tanaka scheme on the vibrational response of elastically supported thick continuously graded carbon nanotube-reinforced annular plates, *Polym Compos*, 2014; 35, 1644-1661.

[35] Tahouneh, V, Yas, MH, Semi-analytical solution for three-dimensional vibration analysis of thick multidirectional functionally graded annular sector plates under various boundary conditions, *J Eng Mech*, 2013, 140, 31-46.

[36] Qian LF, Batra RC, Chen LM. Static and dynamic deformations of thick functionally graded elastic plates by using higher-order shear and normal deformable plate theory and meshless local Petrov–Galerkin method, *Compos Part B* 2004; 35: 685–697.

[37] Liew KM, He XQ, Tan MJ, Lim HK. Dynamic analysis of laminated composite plates with piezoelectric sensor/actuator patches using the FSDT mesh-free method, *Inter J Mech Sci,* 2004; 46: 411–431.

[38] Lanhe W, Hongjun W, Daobin W, Dynamic stability analysis of FGM plates by the moving

least squares differential quadrature method, *Compos Struct,* 2007; 77: 383–394.

[39] Rezaei Mojdehi A, Darvizeh A, Basti A, Rajabi H. Three dimensional static and dynamic analysis of thick functionally graded plates by the meshless local Petrov–Galerkin (MLPG) method, *Eng Anal Bound Elements,* 2011; 35: 1168–1180

[40] Foroutan M, Moradi-Dastjerdi R, Sotoodeh-Bahreini R. Static analysis of FGM cylinders by a mesh-free method, *Steel Compos Struct,* 2012; 12: 1-11.

[41] Mollarazi HR, Foroutan M, Moradi-Dastjerdi R. Analysis of free vibration of functionally graded material (FGM) cylinders by a meshless method, *J Compos Mater* 2012; 46: 507–15.

[42] Foroutan M, Moradi-Dastjerdi R. Dynamic analysis of functionally graded material cylinders under an impact load by a mesh-free method, *Acta Mech,* 2011; 219: 281-90.

[43] Lei ZX, Liew KM, Yu JL. Buckling analysis of functionally graded carbon nanotube-reinforced composite plates using the element-free kp-Ritz method, *Compos Struct,* 2013; 98:160–168.

[44] Lei ZX, Liew KM, Yu JL. Free vibration analysis of functionally graded carbon nanotube-reinforced composite plates using the element-free kp-Ritz method in thermal environment, *Compos Struct,* 2013; 106: 128–138.

[45] Moradi-Dastjerdi R, Momeni-Khabisi H, Dynamic analysis of functionally graded nanocomposite plates reinforced by wavy carbon nanotube. *Steel Compos Struct,* 2016; 22: 277-299.

[46] Moradi-Dastjerdi R, Pourasghar A. Dynamic analysis of functionally graded nanocomposite cylinders reinforced by wavy carbon nanotube under an impact load. *J Vib Control* 2016; 22: 1062-1075.

[47] Moradi-Dastjerdi R, Payganeh G, Rajabizadeh Mirakabad S, Jafari Mofrad- Taheri M, Static and Free Vibration Analyses of Functionally Graded Nanocomposite Plates Reinforced by Wavy Carbon Nanotubes Resting on a Pasternak Elastic Foundation. *Mech Adv Compos Struct,* 2016; 3: 123-135.

[48] Yaghoubshahi M, Alinia MM. Developing an element free method for higher order shear deformation analysis of plates, *Thin-Walled Struct,* 2015; 94: 225–233.

[49] Zhang LW, Lei ZX, Liew KM, An element-free IMLS-Ritz framework for buckling analysis of FG–CNT reinforced composite thick plates resting on Winkler foundations, *Eng Anal Bound Elements,* 2015; 58: 7–17.

[50] Zhang LW, Song ZG, Liew KM, Nonlinear bending analysis of FG-CNT reinforced composite thick plates resting on Pasternak foundations using the element-free IMLS-Ritz method, *Compos Struct,* 2015; 128: 165–175.

[51] Efraim E, Eisenberger M, Exact vibration analysis of variable thickness thick annular isotropic and FGM plates. *J Sound Vib,* 2007; 299: 720–38.

[52] Lancaster P, Salkauskas K, Surface Generated by Moving Least Squares Methods, *Math Comput,* 1981; 37: 141-58.

[53] Hyer MW. 1998, Mechanics of composite materials. McGraw-Hill.

[54] Baferani AH, Saidi AR, Ehteshami H, Accurate solution for free vibration analysis of functionally graded thick rectangular plates resting on elastic foundation. *Compos Struct,* 2011; 93: 1842–53.